LC-PHSM-2003-072
25th August 2003

A Study of Charged Current Triple Gauge Couplings at an $e\gamma$ - collider

K.Mönig, J.Sekaric

Deutsches Elektronen-Synchrotron DESY
Platanenallee 6, 15738 Zeuthen, Germany

Abstract

If there is no light Higgs boson, the interaction among the gauge bosons becomes strong at high energies [$\sim$ 1 TeV]. The effects of strong electroweak symmetry breaking (EWSB) could manifest themselves indirectly as anomalous couplings before they give rise to new physical states like resonances. Here we present a study of the measurement of trilinear gauge couplings looking at the hadronic decay channel of W boson production at an $e\gamma$ - collider. A sensitivity in the range of 10^{-3} to 10^{-4} can be reached depending on the coupling under consideration.

1 Introduction

The measurement of trilinear gauge couplings (TGC) gives us the possibility to study the bosonic sector of the Standard Model (SM). Deviations from the SM as a consequence of anomalous gauge boson interactions indicate a signal of New Physics beyond the SM. The study of such interactions at high energies [~ 1 TeV] is an essential part of the program of Linear Colliders (LC) which includes e^+e^-, $\gamma\gamma$ and $e^-\gamma$ modes. The e^+e^- mode of the LC has been already studied in detail [1] and the sensitivity to the coupling parameters is estimated to be of order 10^{-4}. Estimated errors of couplings in W pair production via $\gamma\gamma$ collisions are also given in [2].

In this study the expected sensitivity for a measurement of the triple gauge couplings in $e^-\gamma \to \nu_e W^-$ at a centre-of-mass energy of 450 GeV is investigated, corresponding to an electron beam energy of 250 GeV. For coupling parameter estimations we assumed that the beam electrons are left-handed. Since the W boson doesn't couples to the right-handed electrons this increases the cross section by a factor of two. The beam photons are right-handed in order to suppress the contribution from the s-channel e-exchange [Fig. 1a]. In this way it's possible to achieve higher sensitivity to the TGCs. The TGC in $e\gamma$-collisions contributes through t-channel W-exchange as it is shown at Fig.1b.

2 Trilinear Gauge Coupling

The trilinear gauge boson vertices, involving only W and γ bosons, can be described by the most general effective Lagrangian as [3]:

$$
\begin{aligned}
\mathcal{L}_{TGC}^{WW} = -ie \Big[& g_1^\gamma V^\mu (W^-_{\mu\nu} W^{+\nu} - W^+_{\mu\nu} W^{-\nu}) + \kappa_\gamma W^+_\mu W^-_\nu V^{\mu\nu} + \frac{\lambda_\gamma}{M_W^2} V^{\mu\nu} W^{+\rho}_\nu W^-_{\mu\rho} \\
& + i g_5^\gamma \varepsilon_{\mu\nu\rho\sigma} [(\partial^\rho W^{-\mu}) W^{+\nu} - W^{-\mu} (\partial^\rho W^{+\nu})] V^\sigma \\
& + i g_4^\gamma W^-_\mu W^+_\nu (\partial^\mu V^\nu - \partial^\nu V^\mu) \\
& - \frac{\tilde{\kappa_\gamma}}{2} W^-_\mu W^+_\nu \varepsilon^{\mu\nu\rho\sigma} V^{\rho\sigma} - \frac{\tilde{\lambda}_\gamma}{2M_W^2} W^-_{\rho\mu} W^+_\nu \varepsilon^{\nu\rho\alpha\beta} V_{\alpha\beta}], \Big]
\end{aligned}
$$

where M_W is the nominal $W^\pm$ mass, V is a photon field, $W^\pm$ are the W fields, and the field tensors are given as $W_{\mu\nu} = \partial^\mu W^\nu - \partial^\nu W^\mu$ and

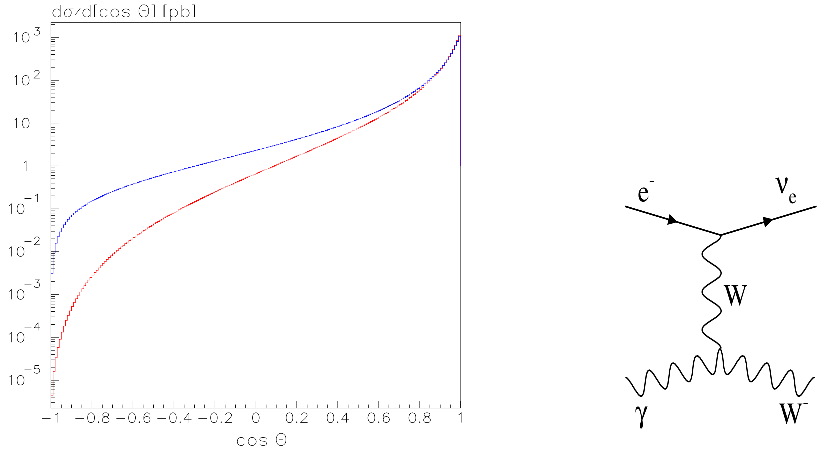

Figure 1: Left: Differential cross-section distributions for two different initial photon helicities - left-handed (blue, upper line) and right-handed (red, lower line). The contribution from the s-channel is visible for left-handed photons leading to a larger cross-section.
Right: Feynman diagram for $e^-\gamma \rightarrow W^-\nu_e$ with TGC contribution only through t-channel W-exchange.

$V_{\mu\nu} = \partial^\mu V^\nu - \partial^\nu V^\mu$. $\varepsilon^{\alpha\beta\gamma\delta}$ is the fully antisymmetric ε-tensor. This Lagrangian describes non-renormalisable and unitarity violating interactions since it is not invariant under the $SU(2)_L \times U(1)_Y$ gauge transformation. The seven coupling parameters of γWW vertices are grouped according to their symmetries as C and P conserving couplings ($g_1^\gamma, \kappa_\gamma$ and λ_γ), C,P violating but CP conserving couplings (g_5^γ) and CP violating couplings ($g_4^\gamma, \tilde{\kappa_\gamma}$ and $\tilde{\lambda_\gamma}$). In the Standard Model all couplings are zero except g_1^γ and κ_γ ($g_1^\gamma = 1, \kappa_\gamma = 1$). Values different from those given in the Standard Model, so called 'anomalous couplings', lead to the corresponding anomalous magnetic dipole moment μ_W and electric quadrupole moment q_W of the W boson:

$$\mu_W = \frac{e}{2M_W}(g_1^\gamma + \kappa_\gamma + \lambda_\gamma)$$

$$q_W = -\frac{e}{2M_W}(\kappa_\gamma - \lambda_\gamma)$$

where $g_1^\gamma = 1$ as gauge invariance requires and possible deviations from SM, denoted as $\Delta\kappa_\gamma$ and λ_γ, arise as a consequence of a New Physics effect.

In this note only the measurement of the C,P conserving couplings, κ_γ, λ_γ, is considered. The other couplings are assumed to take the Standard Model values.

3 Event Selection

In this analysis it was assumed that the energy of the colliding photons is distributed according to the spectrum shown in Fig. 2 [1]. Since the effects of the beam polarisation are minor and not included in Pythia they are not included in the efficiency study. The response of a detector has been simulated with the SIMDET V3 [4], parametric Monte Carlo for the TESLA e^+e^- detector. It includes a tracking and calorimeter simulation and a reconstruction of energy-flow-objects[1]. The acceptance effects of a $\gamma\gamma$ and $e\gamma$ detector are included by taking into account only the energy-flow-objects with a polar angle above 7°.

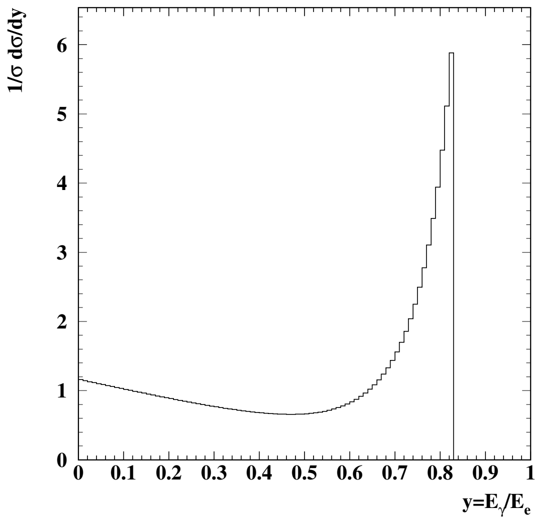

Figure 2: Photon energy spectrum used for the photon beam simulation. The maximum corresponds to $\sim 80\%$ of the electron beam energy.

Sufficiently high cross-section for W boson production [$\sigma_{unpol} \sim 30\,\mathrm{pb}$]

[1]Electrons, photons, muons, charged and neutral hadrons and unresolved clusters that deposit energy in the calorimeters

enables us to separate efficiently signal from background applying several successive cuts. A W boson can decay either into a charged lepton and a neutrino or into a quark - anti-quark pair. This gives two decay channels for single W: the leptonic (BR=0.32) and the hadronic (BR=0.68) decay channel on which this analysis is based. The signal and background events are studied on a sample of events generated with PYTHIA [5]. The energy-flow-objects as hadronisation products are used to reconstruct the signal and background events. The considered backgrounds depend on the two different modes of the $e\gamma$-collider: the real and the parasitic one.

3.1 Real $e\gamma$ mode

The term 'real' is used to point at a collider with one e^- beam and one γ beam. The potential backgrounds for the W signal are those where the final state gives a quark - anti-quark pair. These are:

1. $e\gamma \to eZ$,
   where the Z decays into a quark - anti-quark pair. The preselection cut used to reduce the background contributing to this channel was to reject events whith a high energetic electron ($\geq 100\,\mathrm{GeV}$) in the detector. By this cut $\sim 56\%$ of background events are rejected not affecting the signal efficiency.

2. $\gamma(e^-)\gamma \to q\bar{q}$,
   where one of the initial photons is a bremstrahlung photon.

3.2 Parasitic $e\gamma$ mode

The term 'parasitic' is used to point at a $\gamma\gamma$ collider where the $e\gamma$-collisions are present as a background and we assumed that the directions of incoming particles (e^-, γ) are unknown. The potential backgrounds for the W signal are those where the final state gives a quark - anti-quark pair. Beside those which are relevant for the real $e\gamma$ mode (mentioned above), two additional backgrounds are present:

1. $\gamma\gamma \to WW$,
   where the WW pair decays through the semi-leptonic channel - one W decays through the leptonic channel and another W decays through the hadronic channel. To reduce the background contributing from this

channel in each event we searched for a lepton in the detector with an energy higher than 5 GeV. For these leptons we defined a cone of 30° around their flight directions and summed the energies of all energy-flow-objects (excluding the lepton) inside the cone. If the energy inside the cone was less than 20 GeV the event was rejected. This cut rejects $\sim 57\%$ of the semileptonic WW background events, not affecting the signal efficiency.

2. $\gamma\gamma\rightarrow q\bar{q}$,
   where both initial photons come from beams (real photons).

3.3 Efficiency and background estimations

In order to separate the signal from the background we applied in addition to the vetoes on high energy and isolated leptons cuts on two reconstructed variables, the energy (100 GeV − 250 GeV) and the mass (60 GeV − 100 GeV) of the reconstucted W boson. Successive cuts for real and parasitic $e\gamma$ modes are illustrated in Fig. 3 and in Fig. 5 respectively. Fig. 4 the polar angle distribution of the reconstructed W bosons after all cuts for the real $e\gamma$ mode while Fig. 6 shows the same for the parasitic $e\gamma$ mode.

At 450 GeV, in the real $e\gamma$ mode, the signal is selected with an efficiency of $\sim 90\%$ and a purity of $\sim 82\%$. There are no serious backgrounds for the real $e\gamma$ mode since the background events are distributed out of the kinematical region of the signal.

Concerning the parasitic $e\gamma$ mode the potential background arises from the WW semi-leptonic decay mode. Comparing the signal with the background arising from this channel, signal to background ratio is estimated to be $\sim$ 12:1. Events contributing to this background are mostly hadronic $\tau^{\pm}$ decays where we have not yet tried to isolate the decay products of the τ from the jet. Taking into acount background events from both $e\gamma$ and $\gamma\gamma$ processes the signal is selected with the same efficiency as in the real mode and a purity of $\sim 73\%$.

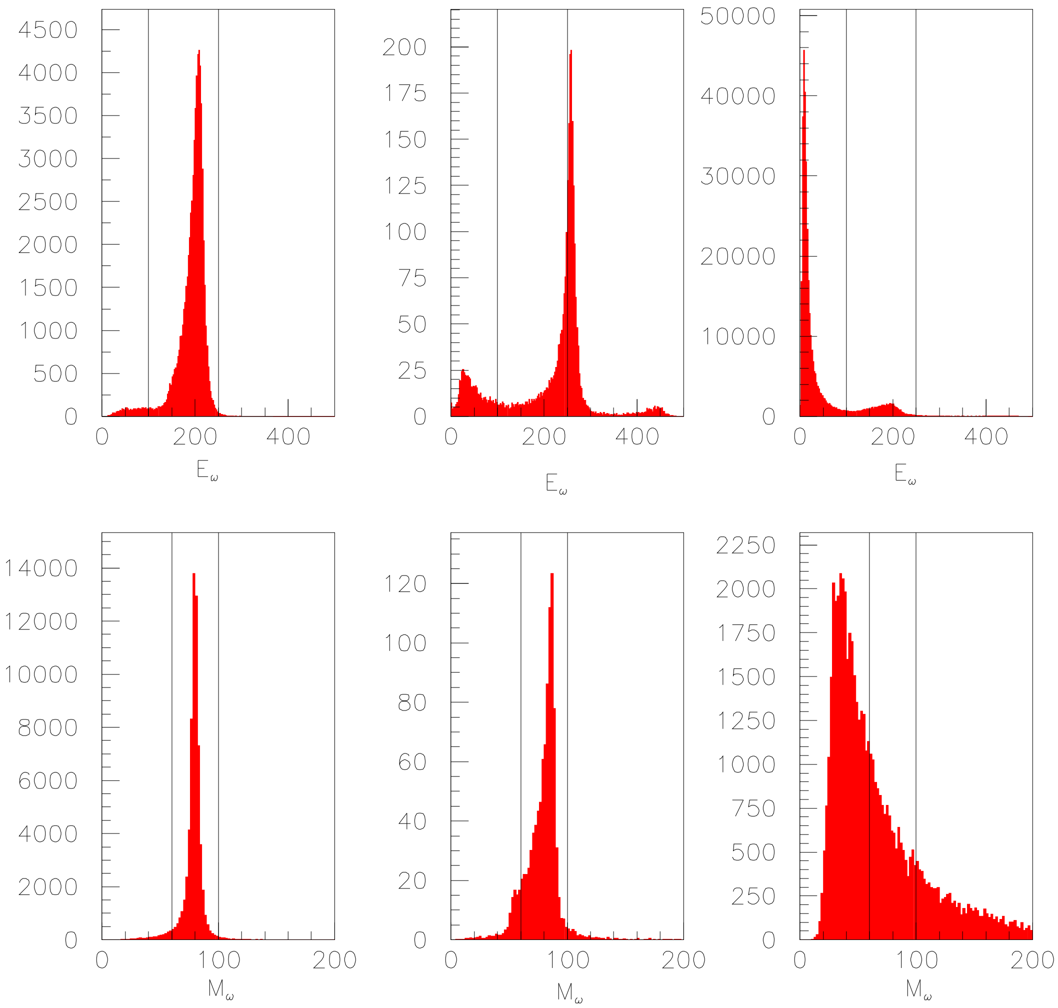

Figure 3: Signal $e^-\gamma \to \nu_e W^-$ [*first column*] to background [*second column ($e\gamma\to eZ$) and third column ($\gamma(e^-)\gamma\to q\bar{q}$) column*] separation - *First row*: energy spectrum of the hadronic final states - the energy cut is imposed in the range between 100 GeV and 250 GeV. *Second row*: mass spectrum of the hadronic final states - the mass cut is imposed in the range between 60 GeV and 100 GeV.

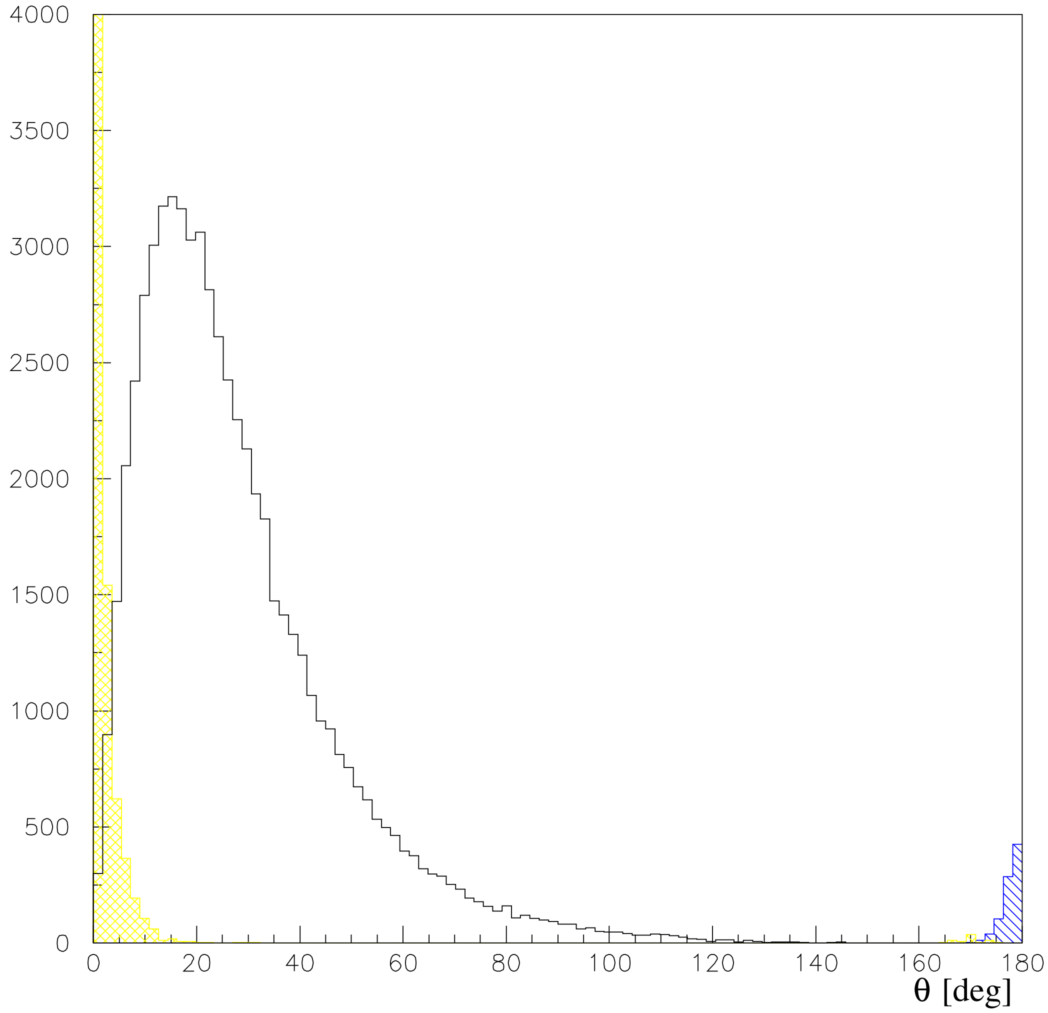

Figure 4: Signal and background for $e\gamma \to W\nu$ in the real $e\gamma$ mode as a function of the W production angle. The white area represents the signal. The hatched contribution on the left is from $\gamma\gamma$ induced processes and the one on the right from $e\gamma \to eZ$. The different processes are normalised to the same luminosity.

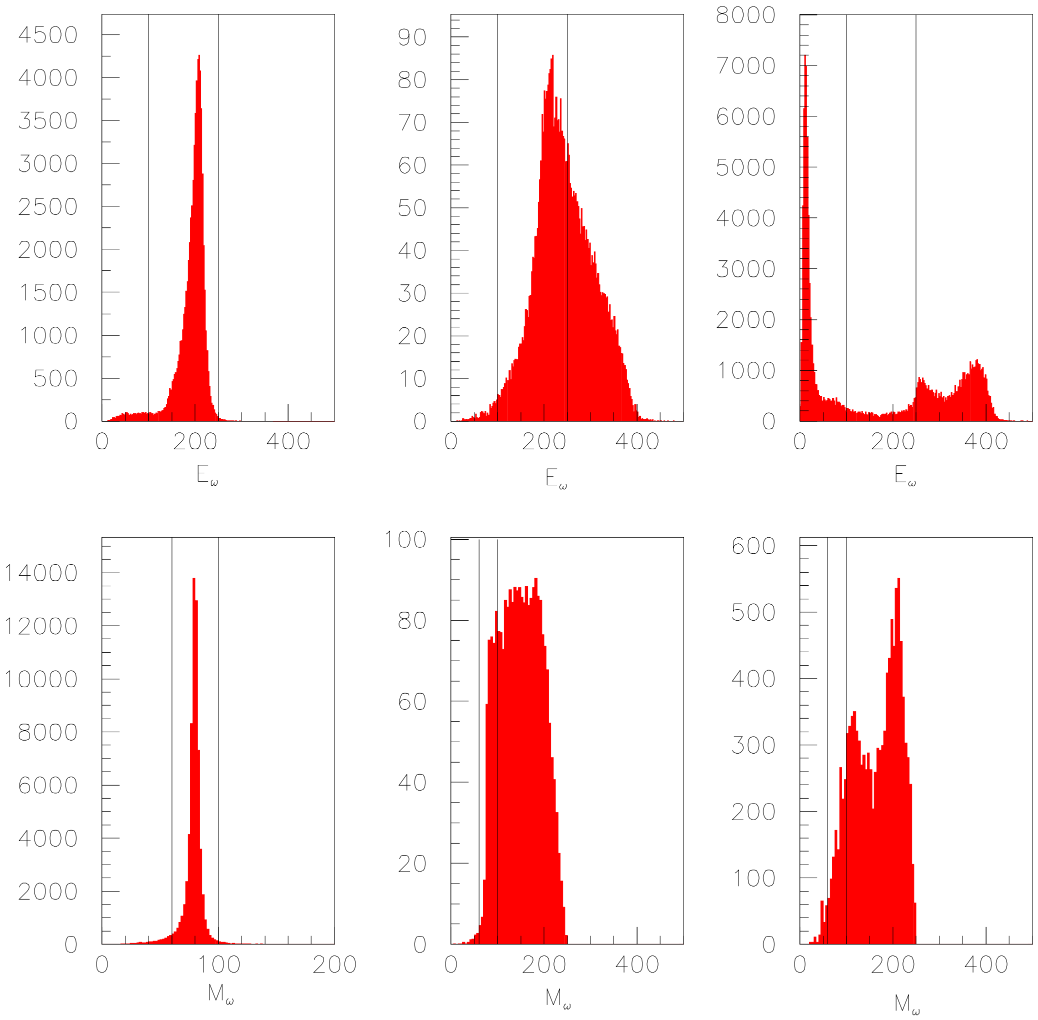

Figure 5: Signal $e^-\gamma\rightarrow\nu_e W^-$ [*first column*] to background [*second column ($\gamma\gamma\rightarrow WW$) and third column ($\gamma\gamma\rightarrow q\bar{q}$) column*] separation - *First row*: energy spectrum of the hadronic final states - the energy cut is imposed in the range between 100 GeV and 250 GeV. *Second row*: mass spectrum of the hadronic final states - the mass cut is imposed in the range between 60 GeV and 100 GeV.

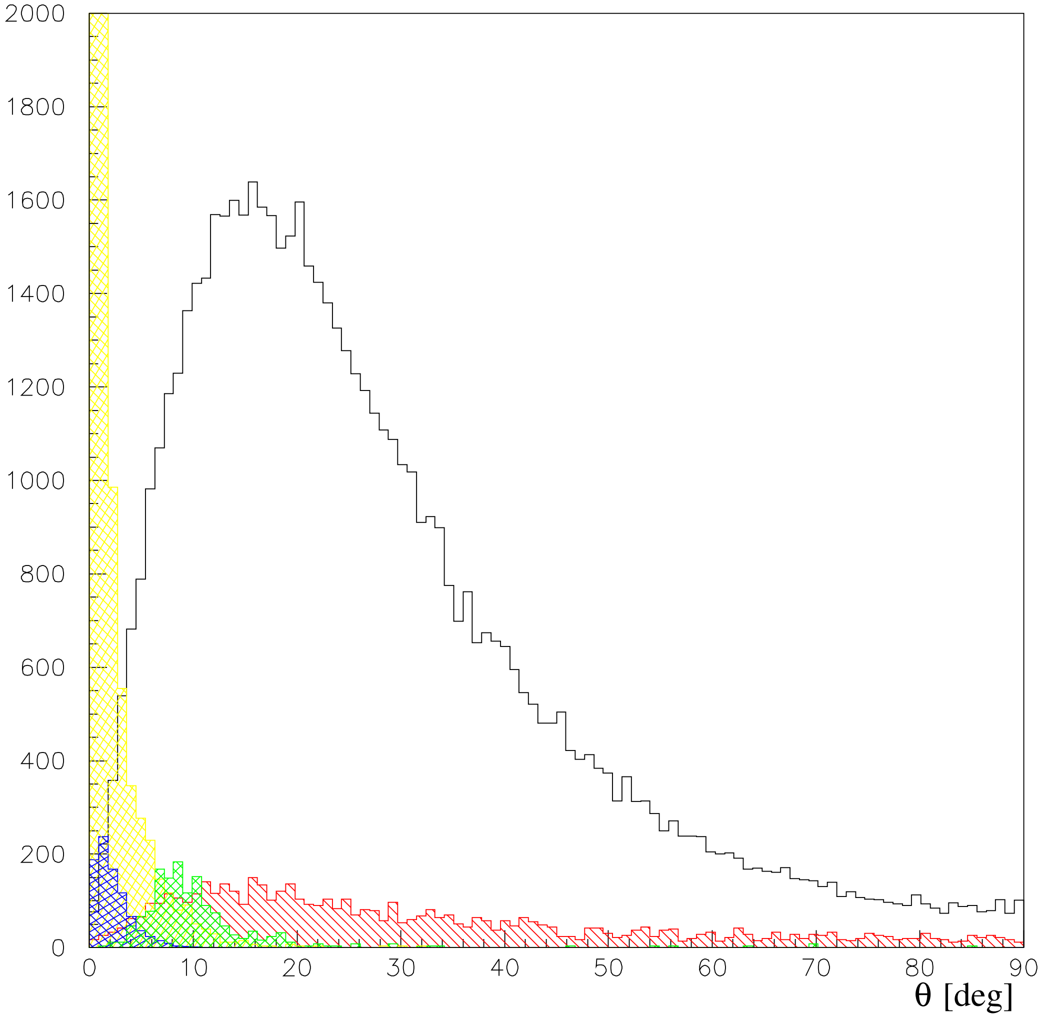

Figure 6: Signal and background for $e\gamma \rightarrow W\nu$ from the parasitic $\gamma\gamma$ running as a function of the W production angle. The white area represents the signal. The light hatched (yellow) contribution on the left is from $\gamma\gamma$ induced processes and the dark hatched (blue) one from $e\gamma \rightarrow eZ$. The additional cross-hatched (green) contribution is from $\gamma\gamma \rightarrow q\bar{q}$ and the singly hatched (red) from $\gamma\gamma \rightarrow WW$. The different processes are normalised to the same luminosity.

4 Observables Sensitive to the Triple Gauge Couplings

Anomalous TGCs can affect both the total production cross-section and the shape of the differential cross-section as a function of the W production angle. The relative contribution of each helicity state of the W boson is also changed in the presence of anomalous couplings [Fig. 7], which in turn affects the distributions of their decay products.

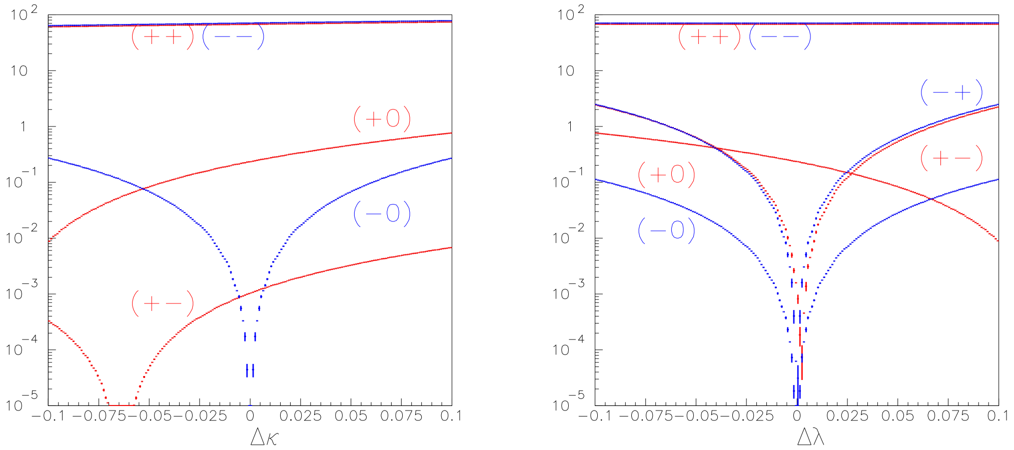

Figure 7: Contribution of different W helicity states for two different initial photon polarisations in the presence of anomalous couplings, $\Delta\kappa_\gamma$ (*left plot*) and λ_γ (*right plot*). $\Delta\kappa_\gamma$: Contribution of (-0) state is suppressed in the SM for while $(-+)$ doesn't contribute at all. λ_γ: Contributions of (-0) and $(-+)$ states are suppressed in the SM. Notation: $(\lambda_\gamma, \lambda_W)$ = (photon helicity, W helicity)

Fig. 8a shows that the differential cross-section distribution in the backward [2] region is more sensitive to the presence of anomalous TGC in the case of right-handed initial photons than for left-handed ones. Fig. 8b shows the different W_L fraction if there are anomalous couplings and in the Standard Model. The production of W_L bosons in the presence of anomalous couplings will differ from the SM especially in the backward region.

[2]Defined as direction of photon beam i.e. the direction opposite to the z-axis

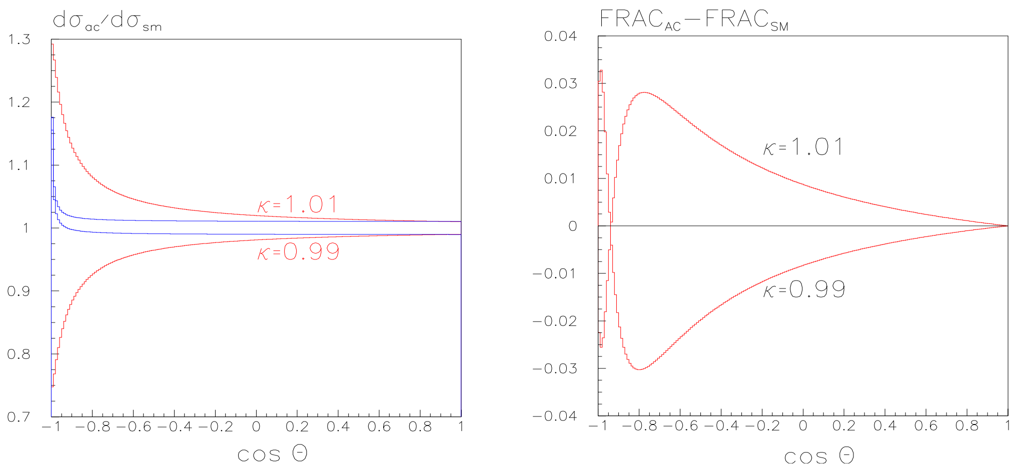

Figure 8: Left (a): Differential cross-section in the presence of anomalous TGCs for both initial photon helicity states - left-handed (blue, inner lines) and right-handed (red, outer lines), normalised to their SM values.
Right (b): Deviation of longitudinal W fraction in presence of anomalous TGCs for $\Delta\kappa_\gamma = \pm 0.01$ from the SM

This behaviour comes from the fact that the information about strong EWSB can be obtained through the study of Goldstone boson interactions which are the longitudinal component of the gauge bosons. Differential cross-sections are calculated on the basis of the formula given in [6] using helicity amplitudes in the presence of anomalous couplings from [7]. The contribution of each W helicity state to the differential cross-section is shown in Fig. 9.

Different W-helicity states are contained in the differential cross-section distribution over the decay angle:

$$\frac{d^2\sigma}{d\cos\theta d\cos\theta_1} = \frac{3}{4}\left[\frac{1}{2}\frac{d\sigma_T}{d\cos\theta}(1+\cos^2\theta_1) + \frac{d\sigma_L}{d\cos\theta}(1-\cos^2\theta_1)\right],$$

where θ denotes the production angle of the W and θ_1 denotes the decay angle. $\frac{d\sigma_T}{d\cos\theta}$ is the differential cross section for the production of transversally polarised W-bosons distributed as $(1+\cos^2\theta_1)$ and $\frac{d\sigma_L}{d\cos\theta}$ is the differential cross section for longitudinal W production, distributed as $\sin^2\theta_1$.

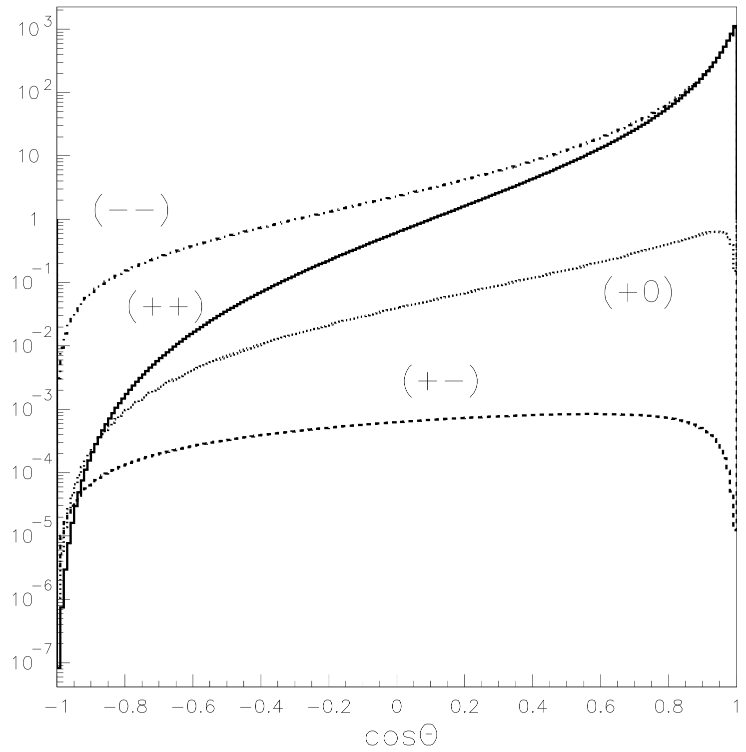

Figure 9: Contribution of each W helicity state for two different initial photon polarisations to the SM differential cross-section. Production of W-bosons with opposite helicity of photons are suppressed in the SM, θ is defined as the angle between the γ beam and the outgoing W. Left sign in parentheses show the initial photon polarisation while right sign in parentheses gives the final W helicity.

5 Fit Method

For the TGC extraction from the reconstructed kinematical variables we used a simple χ^2 fit. A sample of 10^6 SM signal events is generated with the WHIZARD [8] Monte Carlo generator at a centre-of mass energy of 450 GeV that corresponds to an integrated luminosity of $\sim 20\,\mathrm{fb}^{-1}$. The number of events is normalised to that one which correspond to the luminosity of $\sim 110\,\mathrm{fb}^{-1}$ i.e. to the number of events we expect after one year of running of a $e\gamma$-collider. We used 100% polarisation for right-handed photons, $P_\gamma = +1$ and 100% polarisation for left-handed electrons, $P_e = -1$. The matrix element calculations from WHIZARD are used to obtain weights for the reweighting angular distributions as functions of anomalous TGCs.

Each event can be described reconstructing three kinematical variables - W production angle with respect to the e^- beam direction, W polar decay angle $\cos\theta_1$ (angle of the fermion with respect to the W flight direction measured in the W rest frame) and azimuthal decay angle ϕ of the fermion with respect to a plane defined by W and the beam axis. The two decay angles ($\cos\theta_1$, sensitive to the different W helicity states and ϕ, sensitive to the interference between them) in principle describe the direction of the down-type fermion in the rest frame of the W. However, in hadronic W-decays the up- and down-type quarks cannot be separated so that only $|\cos\theta_1$ and $\phi \bmod \pi$ are measured.

The fit is done at generator level assuming full efficiency and at detector level. At detector level, generated events are fragmented, passed through SIMDET and the cuts explained in section 3 are applied. The efficiency using WHIZARD was 80%. This is lower than in the Pythia study, since due the correct description of the W-polarisation in WHIZARD more jets are lost in the forward hole of the detector. However WHIZARD is not yet able to generate events with variable photon energy, so that for the optimisation of the cuts Pythia was preferred. Each Monte Carlo SM event is weighted by a weight

$$R(\Delta\kappa_\gamma, \lambda_\gamma) = 1 + A\Delta\kappa_\gamma + B\Delta{\kappa_\gamma}^2 + C\lambda_\gamma + D{\lambda_\gamma}^2 + E\Delta\kappa_\gamma\lambda_\gamma \qquad (1)$$

where $\Delta\kappa_\gamma$ and λ_γ are the free parameters. The function $R(\Delta\kappa_\gamma, \lambda_\gamma)$, which describes the quadratic dependence of the differential cross-section on the coupling parameters, is obtained in following way: using SM events ($\Delta\kappa_\gamma = \lambda_\gamma = 0$) we recalculated the matrix elements of the events for a set of five different combinations of $\Delta\kappa_\gamma$ and λ_γ values (Table 1):

	R_1	R_2	R_3	R_4	R_5
$\Delta\kappa_\gamma$	0	0	+0.001	-0.001	+0.001
λ_γ	+0.001	-0.001	0	0	+0.001

Table 1: $\Delta\kappa_\gamma$, λ_γ values used to calculate the reweighting coefficients

The resulting recalculated events carry a weight which is given by the ratio of the new matrix element values compared to the SM ones (R_i). The particle momenta are left unchanged. According to the chosen $\Delta\kappa_\gamma, \lambda_\gamma$ combinations from the previous Table one gets:

$$\begin{aligned} R_1 &= 1 + C \mid \lambda_\gamma \mid + D \mid \lambda_\gamma^2 \mid, \\ R_2 &= 1 - C \mid \lambda_\gamma \mid + D \mid \lambda_\gamma^2 \mid, \\ R_3 &= 1 + A \mid \Delta\kappa_\gamma \mid + B \mid \Delta\kappa_\gamma^2 \mid, \\ R_4 &= 1 - A \mid \Delta\kappa_\gamma \mid + B \mid \Delta{\kappa_\gamma}^2 \mid, \\ R_5 &= 1 + A \mid \Delta\kappa_\gamma \mid + B \mid \Delta{\kappa_\gamma}^2 \mid + C \mid \lambda_\gamma \mid + D \mid {\lambda_\gamma}^2 \mid + E \mid \Delta\kappa_\gamma \mid\mid \lambda_\gamma \mid, \end{aligned}$$

where $\mid \Delta\kappa_\gamma \mid = \mid \lambda_\gamma \mid = 0.001$. The coefficients A,B,C,D,E are deduced for each event from the previous five equations as:

$$\begin{aligned} D &= \frac{(M_1 + M_2)}{0.002}, \\ C &= M_1 - 0.001 \cdot D, \\ B &= \frac{(M_3 + M_4)}{0.002}, \\ A &= M_3 - 0.001 \cdot B, \\ E &= \frac{(M_5 - A - C)}{0.001} - (B + D), \end{aligned}$$

with $M_i = \frac{R_i - 1}{0.001}$

Two-dimensional $(\cos\theta, \cos\theta_1)$ and three-dimensional $(\cos\theta, \cos\theta_1, \phi)$ event distributions, integrated over 12 bins of $\cos\theta$, 10 bins of $\cos\theta_1$ and 9 bins of ϕ are weighted by (1) and fitted with MINUIT [9], minimising the χ^2 as a function of κ_γ and λ_γ taking the SM Monte Carlo sample as "data":

$$\chi^2 = \sum_{i=1}^{n}\sum_{j=1}^{n}\sum_{k=1}^{n} \frac{\left(N^{SM}(i,j,k) - n \times N^{\kappa_\gamma,\lambda_\gamma}(i,j,k)\right)^2}{\sigma^2(i,j,k)} + \frac{(n-1)^2}{(\Delta L^2)}$$

where i,j and k run over the angular distributions, $N^{SM}(i,j,k)$ are the "data" which correspond to the SM Monte Carlo sample, $N^{\kappa_\gamma,\lambda_\gamma}(i,j,k)$ is the event distribution weighted by the function $R(\Delta\kappa_\gamma,\lambda_\gamma)$ and $\sigma(i,j,k) = \sqrt{N^{SM}(i,j,k)}$. We also assumed that the total normalisation (efficiency, luminosity, electron polarisation) is only known with a relative uncertainty ΔL. To do this n is taken as a free parameter in the fit and constrained to unity with the assumed normalisation uncertainty.

Per construction the fit is bias-free and thus return always exactly the SM as central values in this study.

A fit performed with data based on the theoretical prediction ([6],[7]) is given in Appendix.

6 Results

The following tables show the estimated statistical errors we expect for the different couplings at $\sqrt{s} = 450\,\text{GeV}$ for two-parameter 2D and 3D fit at generator (Table 2) and detector (Table 3) level, respectively. A two-parameter fit means that both couplings are allowed to vary freely. The correlation between the fit parameters is found to be negligible.

	2D fit			3D fit		
ΔL	1%	0.1%	0	1%	0.1%	0
$\Delta\kappa_\gamma \cdot 10^{-3}$	4.3/5.1	1.0/1.1	0.4/0.5	3.3/3.4	1.0/1.0	0.4/0.4
$\Delta\lambda_\gamma \cdot 10^{-4}$	18/30	15/23	15/22	2.9/3.1	2.7/2.9	2.7/2.9

Table 2: Estimated statistical errors for κ_γ and λ_γ from the two-parameter (2D) and and three-parameter (3D) fit at generator level for the real/parasitic $e\gamma$ mode. The number of events in both modes is normalised to $N_{event} = 4961262$.

The main error of κ_γ is due to the normalisation error for both fit procedures while it doesn't influence λ_γ. Good agreement between real and parasitic modes is achieved for the 3D fit which also results in a higher sensitivity of λ_γ by a factor ~ 7 due to the shape sensitivity of the ϕ distribution to the anomalous λ_γ values. The sensitivity of the ϕ distribution to the anomalous κ_γ is negligible [Fig. 10]. The large difference to the estimated

	2D fit			3D fit		
ΔL	1%	0.1%	0	1%	0.1%	0
$\Delta\kappa_\gamma \cdot 10^{-3}$	4.8/5.0	1.1/1.1	0.5/0.5	3.4/3.5	1.0/1.0	0.5/0.5
$\Delta\lambda_\gamma \cdot 10^{-4}$	26/27	21/21	21/21	3.3/3.4	3.0/3.2	3.0/3.2

Table 3: Estimated statistical errors for κ_γ and λ_γ from the two-parameter (2D) and and three-parameter (3D) fit at detector level for the real/parasitic $e\gamma$ mode. The number of events in both modes is normalised to $N_{event} =$ 3969010.

λ_γ in the 2D fit is due to the flat, non-parabolic shape of the χ^2 function at the minimum [Fig. 11].

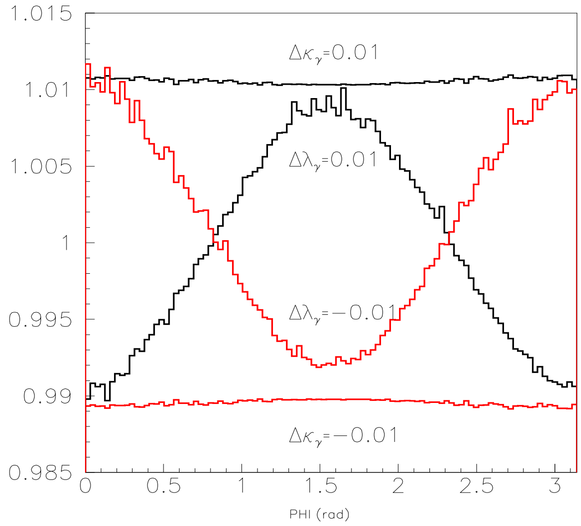

Figure 10: Deviations from SM event distribution over the ϕ angle due to the anomalous couplings $\Delta\kappa_\gamma$ and λ_γ. The sensitivity to the anomalous λ_γ is clearly visible in the shape of the distribution.

Table 4 presents the comparison of the coupling parameter errors estimated by a single-parameter fit for three different types of colliders - $e\gamma$-, $\gamma\gamma$- and e^+e^--collider.

The values in parentheses,($\gamma\gamma$), denote that the ϕ angle as a third dimension is not yet included in the fit.

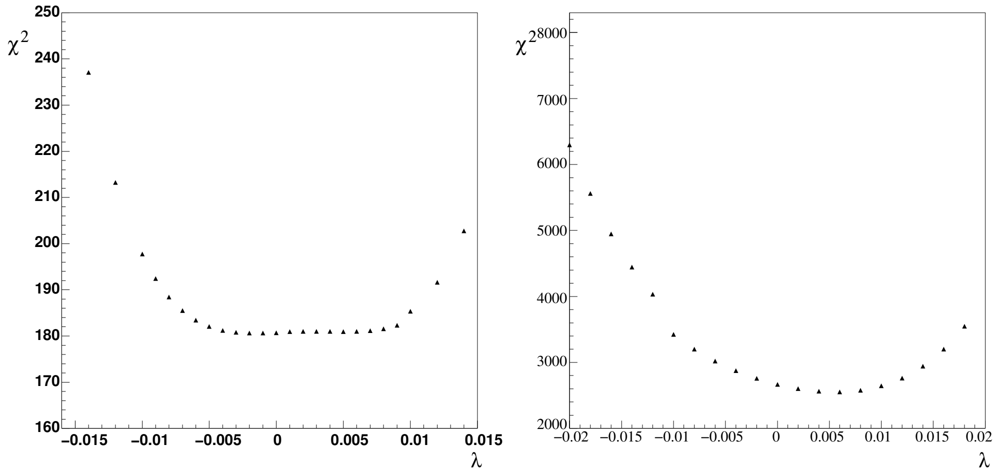

Figure 11: χ^2 distribution as a function of λ_γ for 2D (left) and 3D (right) fit.

	$e\gamma$	$\gamma\gamma$	e^+e^-
ΔL	0.1%	0.1%	
$\Delta\kappa_\gamma \cdot 10^{-4}$	10.1	(6.7)	3.1
$\Delta\lambda_\gamma \cdot 10^{-4}$	2.6	(6.0)	4.3

Table 4: Comparison of the expected errors on κ_γ and λ_γ for three different types of a colliders.

The larger sensitivity to κ_γ is possible to reach with a e^+e^--collider while the $e\gamma$-collider is more sensitive to λ_γ. It's also reasonable to expect that the ϕ distribution in $\gamma\gamma$ will contribute to larger sensitivity than in the e^+e^--collider.

6.1 Systematic errors

6.1.1 Polarisation influence on κ_γ and λ_γ

For a given combination of opposite initial helicities of laser photons and beam electrons it is possible to get highly polarised backscattered photons in a high energy region with a stable polarisation. The possible changes in photon beam polarisation could arise as a consequence of the strong laser wave field.

For TGCs estimation it is important to know the exact polarisation because deviations from the expected ones can fake a contribution from an anomalous coupling. To estimate the systematic error in the TGC measurement coming from the polarisation uncertainty, the polarisation is changed by 1% in the Monte Carlo sample with $P_\gamma = +0.90$. In order to simulate the 1% changes in polarisation the number of events with the opposite polarisation is increased by 10% and mixed with those from the standard sample. The obtained data sample corresponds to data with $P_\gamma = +0.89$.[3]

It was found that for an error on the luminosity of 0.1% we measure κ_γ within an error of 5σ and λ_γ within an error of 1σ. The influence of this systematic error is larger than the statistical error of this test. The photon polarisation thus needs to be known to 0.1% - 0.2% so that κ_γ is not dominated by this systematic error.

6.1.2 Effect of the W-mass measurement

In order to estimate the error coming from the W mass measurement we recalculated the data sample with M_W decreased/increased by 50 MeV reweighting the standard events. The nominal W mass used for Monte Carlo sample was $M_W = 80.419\,\mathrm{GeV}$. As a result of recalculation we get the ratios of matrix element values corresponding for the nominal W mass and for the mass $M_W' = M_W \pm \Delta M_W$. The Monte Carlo sample is weighted by this ratio and fitted as fake data leaving the reference distributions [4] unchanged. The shift in estimated TGCs has shown that the systematic error is of the order of 1σ for both coupling parameters if we assume the error on the luminosity measurement of 0.1%.

7 Conclusion

Due to the fact that the signal is efficiently separated from its background it is possible to estimate the triple gauge couplings with a high precision. We presented that an expected error of the order of 10^{-3} for κ_γ and 10^{-4} for λ_γ is obtained by fit including the ϕ distribution. The contour plot for $\Delta\kappa_\gamma - \lambda_\gamma$ in the generator level fit with no normalisation error is shown

[3] The statistical errors for $P_\gamma = 0.9$ are practically identical to the ones for $P_\gamma = 1$.

[4] Monte Carlo sample with a nominal mass

in Fig. 12. Some sources of systematic errors have been investigated and it was found that the major problem we can expect from uncertainties on the photon beam polarisations which results in a large uncertainty in κ_γ. It's also found that for λ_γ the uncertainty due to the variable photon beam

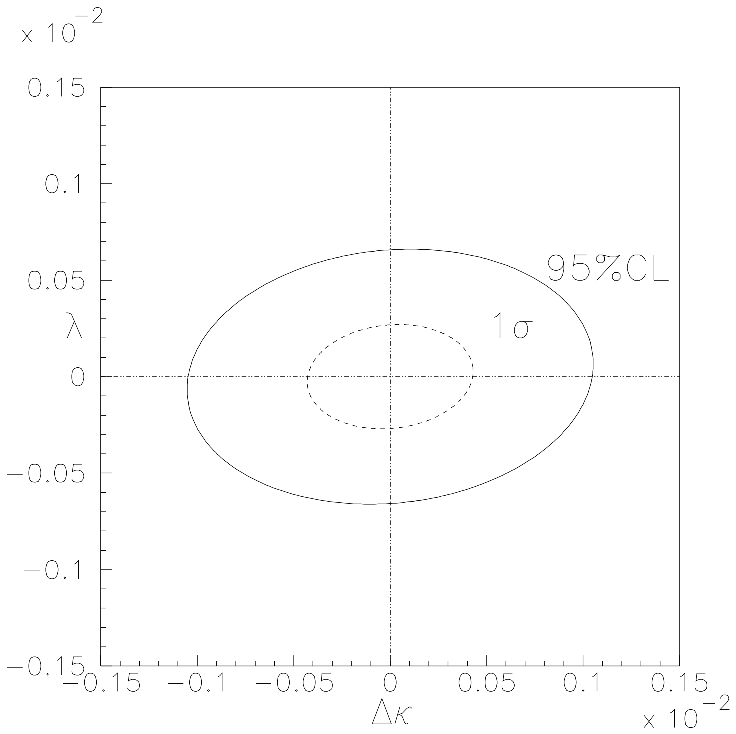

Figure 12: 95% CL and 1σ contours in the $\Delta\kappa_\gamma - \lambda_\gamma$ plane obtained from the 3D fit.

polarisations is negligible. An $e\gamma$ or $\gamma\gamma$ collider is thus the best place for an accurate measurement of λ_γ.

8 Appendix

As an alternative approach the two dimensional event distribution over the production and decay angle Fig. 13 is obtained using the analytical formula from [5] and [6]. Production and decay angle event distributions obtained for a luminosity of $\sim 110\,\text{fb}^{-1}$ are divided into 10×10 bins respectively for parasitic mode and 20×10 bins for real $e\gamma$ mode and fitted with MINUIT [9], minimising the χ^2 function:

$$\chi^2 = \sum_{i=1}^{n}\sum_{j=1}^{n} \frac{\left(N^{SM}(i,j) - n \times N^{\kappa_\gamma,\lambda_\gamma}(i,j)\right)^2}{\sigma^2(i,j)} + \frac{(n-1)^2}{(\Delta L^2)}$$

where i and j are the numbers of bins of corresponding angular distribution. In Table 5 we present the estimations of $\Delta\kappa_\gamma$ and $\Delta\lambda_\gamma$ obtained from the two-parameter fit for data generated from the analytical formula for real and parasitic $e\gamma$ mode. They agree reasonably well with the corresponding results from the reweighting fit (left block of table 4).

ΔL	1%	0.1%	0
$\Delta\kappa_\gamma \cdot 10^{-3}$	4.9/8.4	1.1/1.1	0.4/0.5
$\Delta\lambda_\gamma \cdot 10^{-3}$	2.2/5.9	1.6/2.7	1.5/2.7

Table 5: Estimated statistical errors for κ_γ and λ_γ from the two-parameter 2D fit of the data generated from the analytical formula - real/parasitic $e\gamma$ mode. The number of events is normalised to $N_{event} = 4961262$.

References

[1] TESLA Technical Design report, DESY 2001-011

[2] I.Bozovic-Jelisavcic, K.Mönig, J.Sekaric, *Measurement of Trilinear Gauge Couplings at a $\gamma\gamma$ and $e\gamma$ Collider*, hep-ph/0210308, LCWS August 2002

[3] K.J.F. Gaemers and G.J. Gounaris, Zeit. Phys. **C1** (1979) 259;
K. Hagiwara et al., Nucl. Phys. **B282** (1987) 253.

[4] M.Pohl, J.Schreiber, *SIMDET-Version 3 A parametric Monte Carlo for a TESLA Detector*, DESY 99-030, March 1999

[5] T.Sjöstrand, L.Lönnblad, *PYTHIA 6.1 Physics and Manual*, hep-ph/0108264

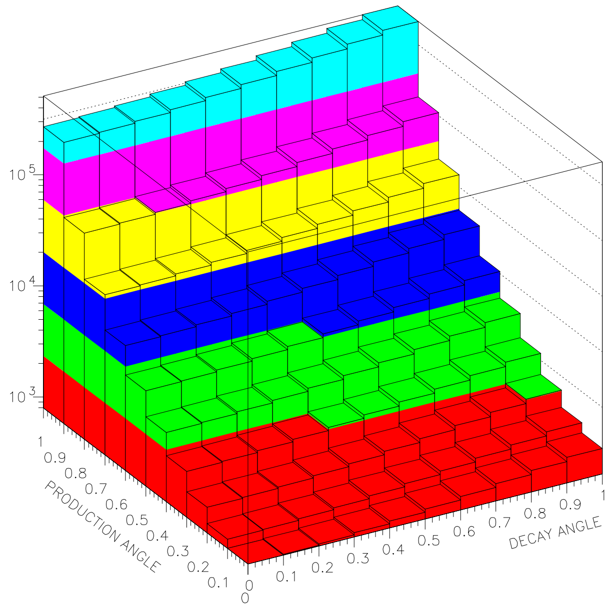

Figure 13: Two dimensional production angle W distribution over the decay angle (10×10 binned distribution).

[6] A.Denner, A.Dittmaier, Nucl.Phys.B398 (1993)236-264

[7] E.Yehudai, Phys.Rev.D44(1991)3434

[8] W. Kilian, *WHIZARD 1.24 A generic Monte Carlo integration and event generation package for multi-particle processes*, LC-tool 2002-039 (revised)

[9] F.James, MINUIT *Function Minimization and Error Analysis, Version 94.1*, CERN Program Library Long Writeup D506